Effect of reactive fumes suppressant DOPO on the chemical composition and performance of asphalt

Zeng, Shangheng; Xu, Shi; Zhang, Tianwei; Duan, Hao; He, Yanheng; Yu, Jianying

DOI
10.1016/j.conbuildmat.2024.137693

Publication date
2024

Document Version
Final published version

Published in
Construction and Building Materials

Citation (APA)
Zeng, S., Xu, S., Zhang, T., Duan, H., He, Y., & Yu, J. (2024). Effect of reactive fumes suppressant DOPO on the chemical composition and performance of asphalt. *Construction and Building Materials*, *443*, Article 137693. https://doi.org/10.1016/j.conbuildmat.2024.137693

Construction and Building Materials 443 (2024) 137693

Contents lists available at ScienceDirect

Construction and Building Materials

journal homepage: www.elsevier.com/locate/conbuildmat

Effect of reactive fumes suppressant DOPO on the chemical composition and performance of asphalt

Shangheng Zeng [a], Shi Xu [b,c], Tianwei Zhang [a], Hao Duan [a], Yanheng He [a], Jianying Yu [a,*]

[a] State Key Laboratory of Silicate Materials for Architectures, Wuhan University of Technology, Wuhan 430070, PR China
[b] Hubei Key Laboratory of Roadway Bridge and Structure Engineering, Wuhan University of Technology, Wuhan 430070, PR China
[c] Faculty of Civil Engineering and Geosciences, Delft University of Technology, Delft 2628 CN, the Netherlands

ARTICLE INFO

Keywords:
Asphalt
Reactive fumes suppressant
DOPO
Properties
Aging resistance

ABSTRACT

9,10-Dihydro-9-oxa-10-phosphorophenanthrene-10-oxide (DOPO), recognized for its role as an efficacious fume suppressant, has been shown to mitigate the emission of noxious vapors emanating from asphalt. However, the comprehensive influence of DOPO on the composition and properties of asphalt had remained unexplored. This study embarked on an in-depth examination of the effects of various DOPO dosages on the chemical composition of asphalt, employing hydrogen nuclear magnetic resonance spectroscopy (^{1}H NMR) alongside an exhaustive analysis of asphalt components. Furthermore, the investigation elucidated the consequences of different DOPO dosages on the physical, rheological properties, and aging resistance of asphalt. The results of ^{1}H NMR and component analysis of asphalt disclosed that DOPO engaged in chemical reactions with the unsaturated groups within the asphalt, catalyzing a metamorphosis of saturates into aromatics and resins. Such chemical transformations were instrumental in augmenting the softening point, viscosity, and rutting propensity of the asphalt while imposing a minimal impact on its penetration and ductility. Post exposure to the thin film oven test (TFOT), pressure aging vessel (PAV), and ultraviolet (UV) aging, the DOPO modified asphalt (DMA) exhibited a diminution in the increment of softening point and viscosity aging index relative to the control asphalt. Furthermore, the DMA showcased enhanced retention rates of penetration and ductility, coupled with substantially reduced shifts in complex modulus and phase angle post-aging, underlining its superior aging resistance. Fourier transform infrared spectroscopy analysis revealed a comparatively slower rate of change in carbonyl and sulfoxide groups in DMA after aging, as opposed to the control asphalt. Notably, DMA exhibited enhanced resistance to UV aging relative to TFOT and PAV aging scenarios, a trait attributable to remarkable UV absorption capabilities of DOPO. Fundamentally, DOPO enhanced the high-temperature performance and aging resistance of asphalt while simultaneously diminishing the emission of noxious fumes.

1. Introduction

Asphalt found extensive applications in pavement construction and roof waterproofing [1–3]. However, Asphalt inevitably generates a large amount of fume during the mixing process of asphalt pavement mixtures and the production process of waterproof materials [4–6]. The primary constituents of asphalt fumes comprised volatile organic compounds (VOCs), polycyclic aromatic hydrocarbons (PAHs), H_2S, and nitrogen oxides [7–10]. The emission of these harmful substances posed a huge threat to the environment and human health [11–14].

The most widely studied asphalt fume suppression method currently was adsorption of the high specific surface area porous material [15–17]. Xiao et al. [18] studied the effect of styrene butadiene styrene (SBS) and active carbon filler on VOCs of asphalt, and the results presented that adding 5 wt% SBS and activated carbon fillers reduced the VOCs content in asphalt by 50 %. Bubenikova et al. [19] investigated the adsorption of Powder Graphite on VOC emissions from expanded polystyrene and showed that Powder Graphite was effective in reducing VOC emissions, with styrene emissions reduced by 14.6 %. Lv et al. [20] prepared UiO-66 MOFs for mitigating fume emissions and found that the addition of 0.9 wt% UiO-66 MOFs could reduce category 1 carcinogens concentrations by 70 %. Wu et al. [16] used zeolite synthesized from red mud and steel slag to reduce VOCs volatilization in asphalt, and the results present that a 5 wt% dosage of synthesized zeolite can reduce the

* Corresponding author.
E-mail address: jyyu@whut.edu.cn (J. Yu).

https://doi.org/10.1016/j.conbuildmat.2024.137693
Received 27 April 2024; Received in revised form 26 June 2024; Accepted 29 July 2024
Available online 5 August 2024

VOCs volatilization of asphalt by 60 %. Tang et al. [21] explored the inhibitory effect of geopolymers on volatile organic compounds and PM emissions from asphalt, and the study showed that the micropores in geopolymers have excellent adsorption capacity for volatile organic compounds and particulate matter emissions from asphalt. Liang et al. [22] developed a new type of asphalt fume suppression mainly composed of basic zinc carbonate. The results showed that a 0.1 wt% inhibitor can reduce 44 % VOCs content and 64 % H_2S content in asphalt fume. Li et al. [23] investigated the effect of kaolin and sepiolite on the fume emission of rubber modified asphalt. The results showed that compared with traditional rubber modified asphalt, the concentration of VOCs in kaolin and sepiolite modified rubber asphalt decreased by 42.26 %. Nonetheless, inorganic adsorbents had limited adsorption capacity and their compatibility with asphalt is inadequate, leading to potential precipitation and diminished asphalt cracking resistance [24,25].

Reactive fume suppressants produce nonvolatile derivatives by reacting with volatile harmful substances in asphalt, consequently mitigating the production of asphalt fume, which not only completely eliminated harmful substances in asphalt, but also eliminated the problem of segregation between suppressants and asphalt [26,27]. In our previous study, we explored the fume suppression effect of 9, 10-Dihydro-9-oxa-10-phosphorophenanthrene-10-oxide (DOPO) on asphalt, and the results showed that at 180 °C, the content of H_2S and VOCs of asphalt with 1 wt% DOPO decreased by 84.2 % and 96.9 %, respectively, which may be due to fact that the reactivity of the P-H bond in DOPO with volatile unsaturated alkanes, aromatic hydrocarbon derivatives, and sulfides present in the asphalt, leading to a decrease in the generation of asphalt fume[28]. Nevertheless, previous studies have exclusively examined the influence of DOPO on asphalt volatiles, with limited clarity on the effect of varying DOPO dosages on the composition of asphalt. Furthermore, the effects of DOPO on the physical and rheological properties of asphalt remain ambiguous. In addition, because DOPO has excellent ultraviolet absorption capacity, it has very high anti-aging potential, so the effect of DOPO on asphalt aging is very valuable [29,30].

In this study, the effect of DOPO with varying dosages on the chemical composition, physical, rheological and anti-aging performance of asphalt was studies, respectively. Firstly, DOPO modified asphalt (DMA) with varying dosages was prepared. Then, the chemical composition changes of DMA with different dosage were characterized through nuclear magnetic resonance (NMR) and column chromatography. The effect of DOPO on the physical and rheological properties as well as the anti-aging performance of DMA under thin film oven test (TFOT), pressure aging vessel (PAV) and ultraviolet (UV) aging was investigated. Finally, the mechanism anti-aging performance of DMA was then explored.

2. Materials and methodology

2.1. Materials

The properties of Pen 60/80 asphalt, produced by China National Petroleum Corporation, were detailed in Table 1. Additionally, 9,10-dihydro-9-oxa-10-phosphophenyl-10-oxide with a purity of 98 % was obtained from Aladin Biochemical Technology Co., Ltd, China.

Table 1
Physical properties of the asphalt.

Physical properties	Test value
Penetration (25 °C, 0.1 mm)	69
Softening point (°C)	48.3
Ductility (10 °C, cm)	71
Viscosity (60 °C, Pa s)	328

2.2. Preparation of DMA

DMA was synthesized using the melt blending method. Specifically, 200 g of asphalt was loaded into three-necked flasks at 165 °C. DOPO was added at varying dosages (0, 0.3 wt%, 0.6 wt%, and 0.9 wt% of asphalt) and subjected to mixing at 165 °C for 45 min at 800 rpm to yield DMA.

2.3. Aging simulation test of the asphalt

To replicate the aging effect of DMA, in this research, short-term aging of DMA was simulated by thin film oven test (TFOT), and long-term aging of DMA was simulated by pressure aging container (PAV) and ultraviolet aging (UV) tests.

DMA for the TFOT were heated in the oven for 5 h at 163 °C according to ASTM D1754.

DMA after TFOT were subjected to PAV aging tests. The standard aging procedure of 100 °C, 2.1 MPa and 20 h for the PAV was used according to ASTM D 6521.

DMA after TFOT were subjected to UV aging tests. DMA was exposed to UV light for 7 days in an accelerated aging oven under conditions of 50 °C, 40 W/m^2 radiation intensity, and 365 nm ultraviolet wavelength [31].

2.4. ^1H NMR

The hydrogen atoms in the asphalt samples were analyzed using ^1H NMR (Bruker AVANCE III HD, Switzerland). Dissolve 6 mg of DMA in 6 ml of deuterated chloroform ($CDCl_3$) solvent before analysis.

2.5. Asphalt chemical components testing

The components of DMA with different dosages were divided into saturate (S), aromatic (A), resin (R), and asphaltene (A). This testing included the following steps, according to ASTM D4124–2001 standard: 1) 1 g ± 0.1 g of DMA was dissolved in n-hexane to separate and obtain asphaltene. 2) Separate the filtrate obtained from 1) using a 1:1 mixture of n-hexane, toluene, and saturated toluene with ethanol in a glass chromatography column of activated alumina, to obtain saturate, aromatic, and resin; 3) Distill the corresponding filtrate to obtain the components of DMA. 4) Weigh the components of DMA obtained, repeat the experiment twice, and take the average value

2.6. Physical properties test

The physical properties of DMA, including softening point, viscosity (60 °C), penetration (25 °C), and ductility (15 °C), were measured in accordance with ASTM standards D36, D4402, D5, and D113–86, respectively.

2.7. Dynamic Shear Rheometer (DSR) test

According to ASTM D8189–19, the complex modulus of DMA before and after aging was determined using a dynamic shear rheometer (MCR-101, Anton Paar, Austria). In this experiment, DMA were subjected to temperature scanning tests at a fixed frequency of 10 rad/s and a temperature increment of 2 °C/min in the range of 30 °C to 80 °C.

2.8. UV–visible spectrophotometer

Evaluate the light blocking performance of DOPO in the wavelength range of 200–800 nm using a UV visible spectrophotometer (Lambda 750 s, PerkinElmer, USA).

2.9. FTIR

FTIR spectrometry (Nexus , Thermo Nicolet Corp. , USA) was utilized to evaluate the variations in chemical functional groups of DMA under varying conditions aging. Mixed solution of DMA was prepared by dissolving it in carbon disulfide; then, it was deposited onto KBr and dried to form a thin film. The observed spectral range was 4000–400 cm^{-1}.

2.10. Experimental flowchart

The experimental arrangement for testing was illustrated in the process chart shown in Fig. 1.

3. Result and discussion

3.1. Effect of DOPO on the chemical composition of asphalt

3.1.1. ^1H NMR analysis

The ^1H NMR spectra of DMA elucidating the interaction of DOPO and asphalt at incremental dosages were depicted in Fig. 2. As delineated therein, the resonant peak corresponding to the hydrogen proton, associated with the β carbon on the aromatic ring within the control asphalt, was discerned at δ = 1.0–2.0 ppm. Concurrently, the spectral features at δ = 2.0–4.0 ppm were ascribed to the hydrogen proton adjacent to the α carbon of the aromatic ensemble in DMA. The defining resonances of the hydrogen protons, situated on the biphenyl rings in both the asphalt and DOPO, emerged distinctly at 7.0–8.0 ppm. Furthermore, the peak manifesting at δ = 8.6 ppm was attributed to the hydrogen protons bonded to the phosphorus atom within the DOPO structure[32,33].

The varying hydrogen contents in DMA with different dosages of DOPO were summarized in Table 2. An insightful examination of this table revealed an augmentation in the H_{ar} content of 0.3 wt% DMA, ascending from 2.2 % to 3.5 % compared to the control asphalt. This trend of increment persisted with enhanced DOPO integration, where the H_{ar} content in DMA escalated to 8.1 % at a DOPO dosage of 0.9 wt%. This uptrend was attributed to the pronounced H_{ar} signature in DOPO, culminating in its amplified representation in DMA. In a parallel vein, there was a notable elevation in the Hα constituent within DMA, surging from 14.9 % in 0.3 wt% DMA to 21.2 % in 0.9 wt% DMA. Such an ascension was potentially ascribable to the interplay between the unsaturated linkages in asphalt and the P-H bonds in DOPO, engendering a reduction in the unsaturation of asphalt while concurrently enriching its functional group. Moreover, the negligible presence of P-H bonds in DMA, irrespective of DOPO, signified the reaction of these bonds in DOPO with the asphalt.

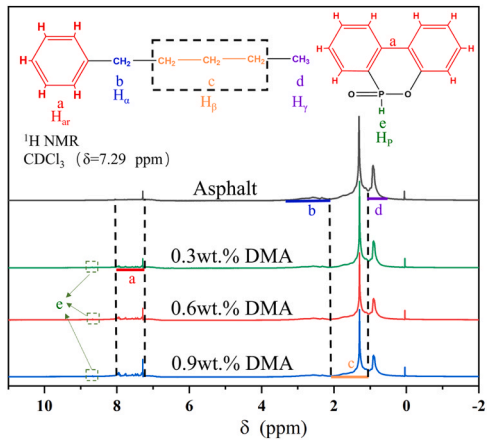

Fig. 2. ^1H NMR spectrums of DMA with varying dosages of DOPO.

Table 2
Different hydrogen atom content of DMA.

	$H_α$	$H_β$	$H_γ$	H_{ar}	H_P
Asphalt	0.128	0.552	0.298	0.022	0
0.3 wt%DMA	0.149	0.531	0.284	0.035	0.001
0.6 wt%DMA	0.180	0.503	0.258	0.058	0.001
0.9 wt%DMA	0.212	0.475	0.232	0.081	0

3.1.2. SARA analysis

SARA components of DMA with different dosages of DOPO was depicted in Fig. 3. As shown in Fig. 3 that there were significant differences in the SARA components of DMA with different DOPO dosages. With the incremental dosage of DOPO, there was a discernible decrement in the saturates of DMA, juxtaposed with a concomitant augmentation in its aromatics and resins. Specifically, in the absence of DOPO, the DMA exhibited a saturate content of 16.56 %, an aromatic content of 43.14 %, a resin content of 29.51 %, and an asphaltene content of 10.79 %. When the dosage of DOPO was 0.3 wt%, the saturate content diminished to 14.32 %, while the aromatic and resin content escalated to 44.83 % and 30.03 % respectively, with the asphaltene content remaining relatively stable at 10.82 %. These transformations were attributable to the chemical reaction between DOPO and asphalt, facilitating a transmutation of saturates within DMA into aromatic and resin constituents. Advancing this narrative, at a DOPO dosage of 0.6 wt %, the saturate content of DMA decreased further to 12.65 %, while the aromatic and resin content ascended to 45.12 % and 31.20 %

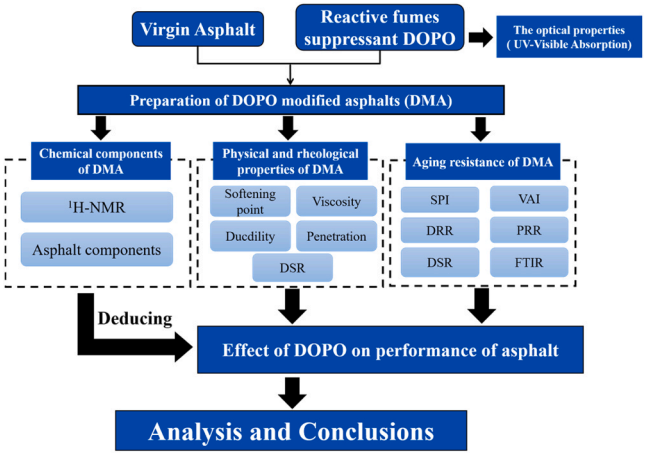

Fig. 1. Research process chart.

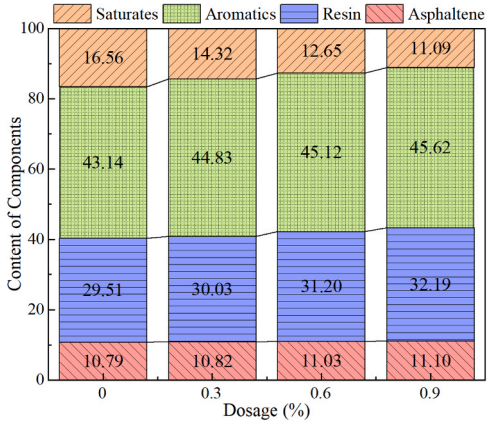

Fig. 3. SARA components of DMA with varying dosages of DOPO.

respectively. The asphaltene content at this juncture was recorded at 11.03 %. Escalating the DOPO dosage to 0.9 wt% precipitated a reduction in the saturate content to 11.09 %, while elevating the aromatic and resin contents to 45.62 % and 32.19 % respectively, with the asphaltene content slightly increasing to 11.10 %.

3.2. Effect of DOPO on physical and rheological property of asphalt

3.2.1. Physical property of DMA

3.2.1.1. Softening point. Fig. 4 delineated the variation in the softening point of DMA as influenced by incremental dosages of DOPO. As elucidated in Fig. 4, there was a discernible escalation in the softening point of DMA, ascending from 48.5 °C to 49.3 °C with the integration of 0.3 wt % DOPO, marking an enhancement of 0.8 °C. This augmentation was ostensibly attributed to the chemical interplay between DOPO and the asphalt, manifesting as a reduction in the saturate alongside an elevation in the aromatic and resin within the asphalt. With progressive DOPO enrichment, there was a noticeable continuous increase in the softening point of DMA. At a DOPO dosage of 0.9 wt%, the softening point further escalated to 50.3 °C, reflecting a substantial increase of 1.8 °C relative to the control asphalt specimen. This trend was likely indicative of a more profound and extensive reaction between DOPO and asphalt, particularly at elevated DOPO dosages, influencing the thermal properties.

3.2.1.2. Viscosity. Fig. 5 depicted the viscosity of DMA with varying dosages of DOPO. The viscosity of DMA witnessed a subtle rise from 332 Pa·s to 356 Pa·s with the incorporation of 0.3 wt% DOPO, indicating a direct correlation between DOPO content and viscosity. Further escalation was observed as DOPO dosage intensifies; at 0.6 wt%, the viscosity ascended to 377 Pa·s, surpassing the control by 45 Pa·s. At the dosage of 0.9 wt% DOPO, the viscosity reached 391 Pa·s.

3.2.1.3. Ductility. The ductility of DMA with varying dosages of DOPO were presented in Fig. 6. illustrating a marginal influence. At a dosage of 0.3 wt% DOPO, the ductility of DMA was 70 cm, similar to that of the control asphalt. However, with the increase of DOPO doping, the ductility of DMA slightly decreased. At a dosage of 0.6 wt% DOPO, the ductility of DMA was 69 cm, which was only 1 cm less than that of control asphalt. At a dose of 0.9 wt% DOPO, the ductility of DMA was also 69 cm. This may be because the content of most of the stable saturate, which were not easily susceptible to oxidation or volatile, were not reduced and the asphaltene content had not increased, although some saturate in DMA were converted into aromatic and resin after DOPO reacted with asphalt, resulting in almost no change in the ductility of DMA.

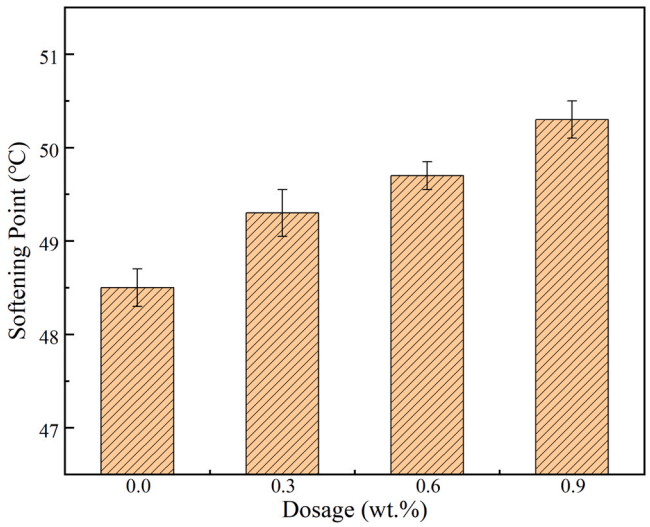

Fig. 4. Softening point of DMA with varying dosages of DOPO.

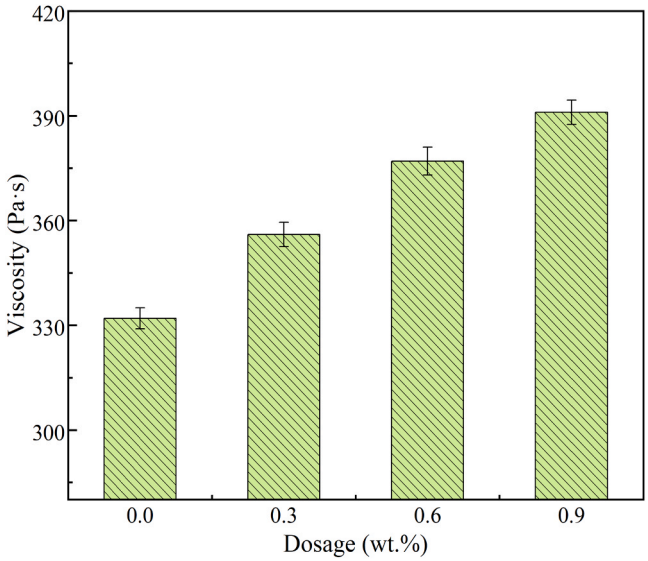

Fig. 5. Viscosity of DMA with varying dosages of DOPO.

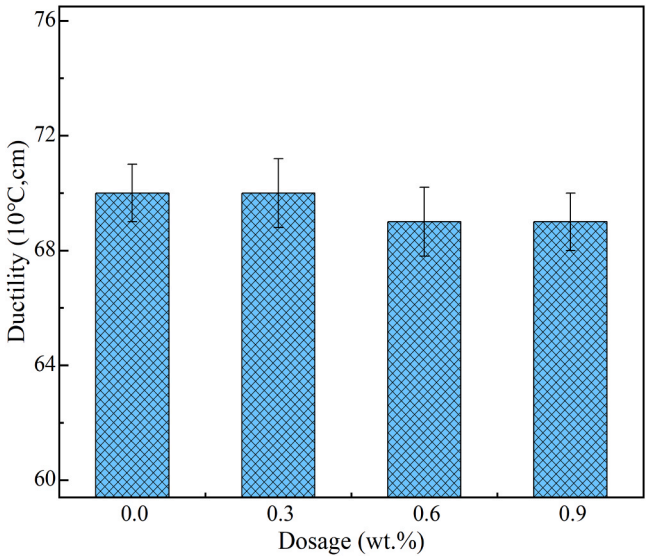

Fig. 6. Ductility of DMA with varying dosages of DOPO.

3.2.1.4. Penetration. The penetration of DMA with various dosages of DOPO were depicted in Fig. 7. Fig. 7 illustrated that the penetration of DMA was slightly lower than that of control asphalt. Specifically, at a dosage of 0.3 wt% DOPO, the penetration of DMA measured 67dmm, which was 1dmm lower than that of control asphalt. Furthermore, an increase in DOPO doping led to a slight decrease in the penetration of DMA. At a dosage of 0.6 wt% DOPO, the penetration of DMA was 66 dmm, indicating a 2dmm reduction compared to control asphalt. At a dosage of 0.9 wt% DOPO, the penetration of DMA was 65dmm, reducing the penetration of control asphalt by only 3 dmm.

3.2.2. Rheological properties of DMA

Fig. 8 meticulously delineated the relationship between the complex modulus, the phase angle-temperature, and the variegated dosages of DOPO in DMA asphalt, whilst Fig. 9 elucidated the corresponding ramifications on the rutting factors of DMA. The viscoelastic properties

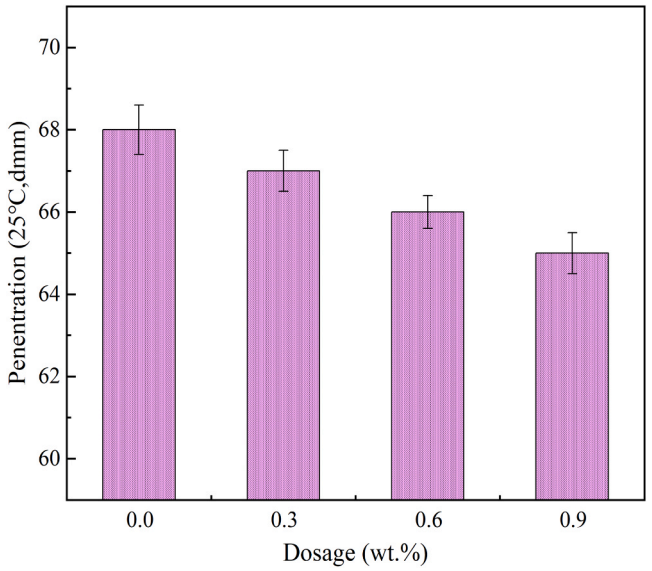

Fig. 7. Penetration of DMA with varying dosages of DOPO.

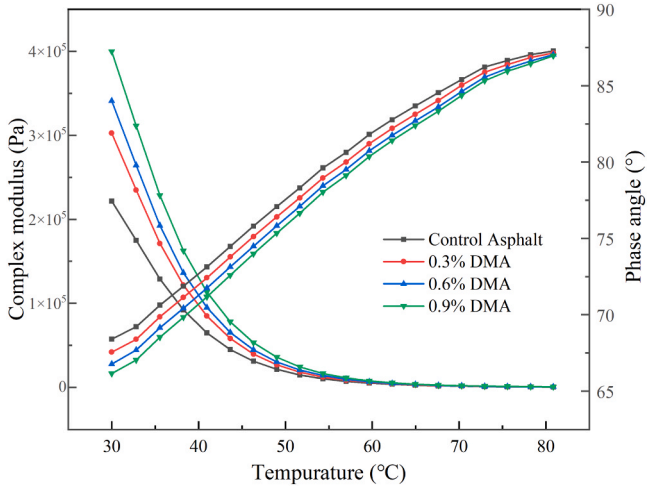

Fig. 8. Complex modulus and phase angle-temperature relationship of DMA with different dosages of DOPO.

of the asphalt were quantified by the phase angle (δ), where elevated values signify diminished elasticity and augmented viscosity. The graphical representation in Fig. 8 unveiled a conspicuous trend: an escalation in the complex modulus (G*) and a diminution in δ across all specimens, indicative of an intensification in viscosity and a decrement in elasticity concomitant with an upsurge in temperature. Intriguingly, the δ value for DMA was consistently lower than that of the control asphalt, insinuating that the DOPO interaction catalyzes a transformative shift in DMA from a viscous to a more elastic state. The G* metric for DMA manifested a uniform trend across disparate DOPO dosages, presumably as a consequence of the reaction of DOPO and asphalt. Specifically, at DOPO dosages of 0.3 wt%, 0.6 wt%, and 0.9 wt %, the G* values for DMA at 30 °C were markedly 36.5 %, 53.7 %, and 80.3 % superior to the control asphalt, respectively. Complementary to this, Fig. 9 accentuated that DOPO fortification enhanced the resistance of asphalt binder to rutting. When juxtaposed with the control, the critical rutting temperatures for DMA at 0.3 wt%, 0.6 wt%, and 0.9 wt% escalated by 1.18, 1.97, and 2.95, respectively. Such enhancements were attributable to the diminished saturate content and the augmented aromatic and resin content within DMA, consequently attenuating its

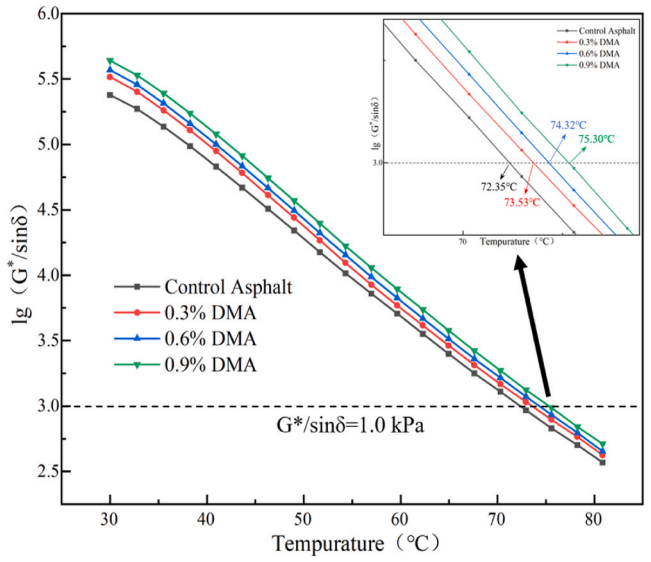

Fig. 9. Rutting factors of DMA with varying dosages of DOPO.

thermal rheological viscoelasticity.

3.3. *Effect of DOPO on anti-aging performance of asphalt*

3.3.1. *UV–visible spectrophotometer of DOPO*

Fig. 10 illustrated the absorbance of DOPO in both the ultraviolet and visible light ranges. The absorbance of DOPO followed a specific trend with respect to wavelength within the 200–450 nm range. Initially, it increased and then decreased as the wavelength increases. Notably, DOPO exhibited the strongest UV absorption peak near a wavelength of 300 nm, thus confirming its exceptional ability to shield against harmful UV radiation. This finding underscores the potential of DOPO as an effective UV protective agent.

3.3.2. *Physical properties of DMA after aging*

3.3.2.1. Softening point increment (SPI). The aging resistance of DMA was evaluated using the SPI before and after aging, with the calculation formula expressed as follows:

$$SPI = Softening\ point_{after\ aging} - Softening\ point_{before\ aging} \quad (6)$$

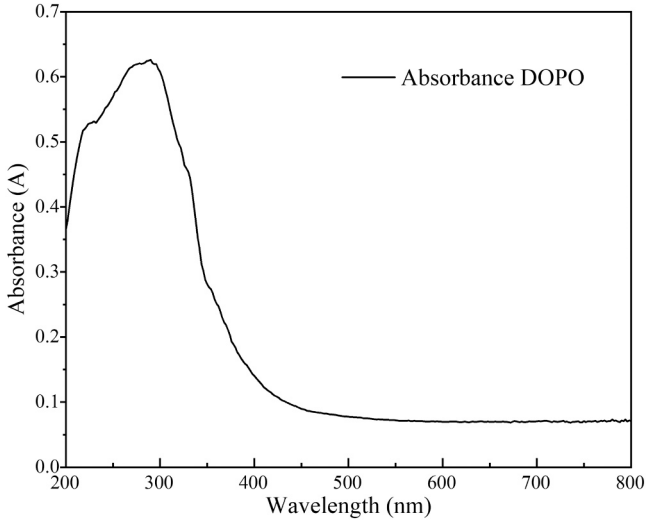

Fig. 10. UV-Visible Absorption curves of DOPO.

The SPI of DMA with different dosages of DOPO after TFOT, PAV and UV aging were presented in Fig. 11. It was worth noting that the trend of SPI changes after TFOT, PAV and UV aging remained consistent at different DOPO dosages, although significant difference in SPI can be observed between the three aging methods. In addition, the SPI of DMA significantly decreased after adding DOPO. Specifically, the SPI of control asphalt after TFOT, PAV, and UV aging were 4.4 °C, 4.8 °C, and 5.7 °C, respectively. However, after TFOT, PAV and UV aging, the SPI of DMA with 0.3 wt% DOPO decreased to 3.7 °C, 4.0 °C and 4.4 °C respectively, which may be attributed to the reaction of DOPO and asphalt forming more stable components in DMA and the functional groups susceptible to oxidize in asphalt decreased, thus improving its anti-aging performance. As the dosage of DOPO increased, the SPI of DMA gradually decreased. When the DOPO content was 0.6 wt%, the SPI of DMA after TFOT, PAV and UV aging decreased to 3.3 °C, 3.5 °C, and 3.8 °C, respectively. It was worth noting that the SPI of DMA with 0.9 wt% DOPO after TFOT, PAV, and UV aging were only 2.8 °C, 3.0 °C, and 3.2 °C, respectively. In summary, the higher the DOPO content, the better the anti-aging performance of DMA.

3.3.2.2. Viscosity aging index (VAI). The aging resistance of DMA was assessed using the VAI before and after aging, with the following calculation formula:

$$VAI = \frac{\text{Viscosity value}_{\ after\ aging} - \text{Viscosity value}_{before\ aging}}{\text{Viscosity value}_{before\ aging}} \quad (7)$$

The VAI values of DMA at different dosages of DOPO under three aging conditions were depicted in Fig. 12. It was observed from the figure that the VAI of DMA decreased significantly after the addition of DOPO. Specifically, the VAI of control asphalt after TFOT, PAV and UV aging was 8.7 %, 11.2 % and 14.0 % respectively, while the VAI of DMA with 0.3 wt% DOPO decreased to 6.6 %, 8.5 % and 11.2 % respectively, which may also be that more stable components had formed in DMA and the UV absorption capacity of DOPO had improved its anti-aging performance. As the dosage of DOPO increased, the VAI of DMA gradually decreased. When the DOPO content was 0.6 wt%, the VAI of DMA after TFOT, PAV, and UV aging decreased to 3.3 %, 3.5 %, and 3.8 %, respectively, while the VAI of DMA with 0.9 wt% DOPO after TFOT, PAV, and UV aging were only 2.8 %, 3.0 %, and 3.2 %, respectively.

3.3.2.3. Ductility retention rate (DRR). The aging resistance of DMA was assessed using the DRR before and after aging, with the following calculation formula:

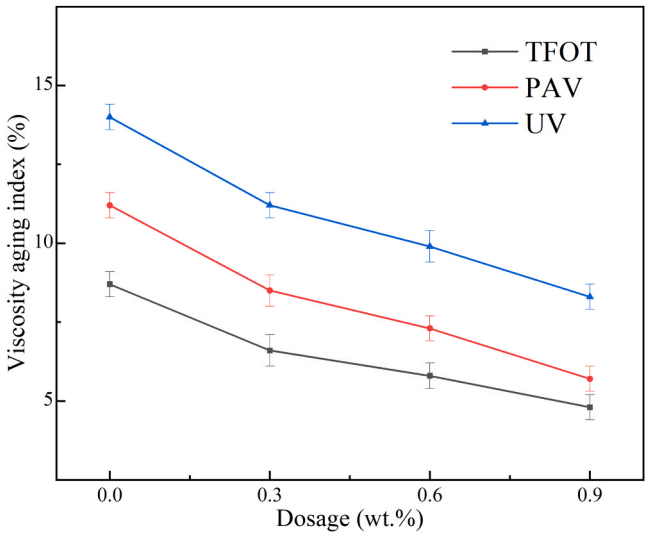

Fig. 12. VAI of DMA with varying dosages of DOPO.

$$DRR = \frac{Ductility_{after\ aging}}{Ductility_{before\ aging}} \times 100\% \quad (8)$$

The DRR of DMA at different dosages of DOPO after TFOT, PAV, and UV aging were presented in the Fig. 13. It can be seen from Fig. 13 that the addition of DOPO significantly increased the ductility of DMA. The DRR of control asphalt after TFOT, PAV, and UV aging were 77.4 %, 76.3 %, and 75.0 %, respectively, while the DRR of DMA with 0.3 wt% DOPO increased to 82.1 %, 80.0 %, and 79.5 %, respectively, which may also be attributed to the more stable components in DMA and the UV absorption ability of DOPO. As the dosage of DOPO increased, the DRR of DMA gradually increased. When the DOPO content was 0.6 wt%, the DRR of DMA after TFOT, PAV, and UV aging increased to 84.9 %, 82.4 %, and 81.7 %, respectively, while the DRR of DMA with 0.9 wt% DOPO content increased to 86.2 %, 84.0 %, and 83.5 % after TFOT, PAV, and UV aging, respectively.

3.3.2.4. Penetration retention rate (PRR). The aging resistance of DMA was assessed using the PRR before and after aging, with the following calculation formula:

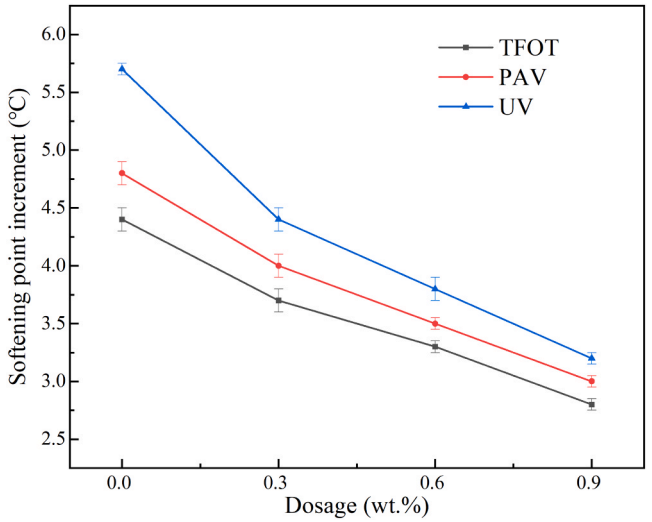

Fig. 11. SPI of DMA with varying dosages of DOPO.

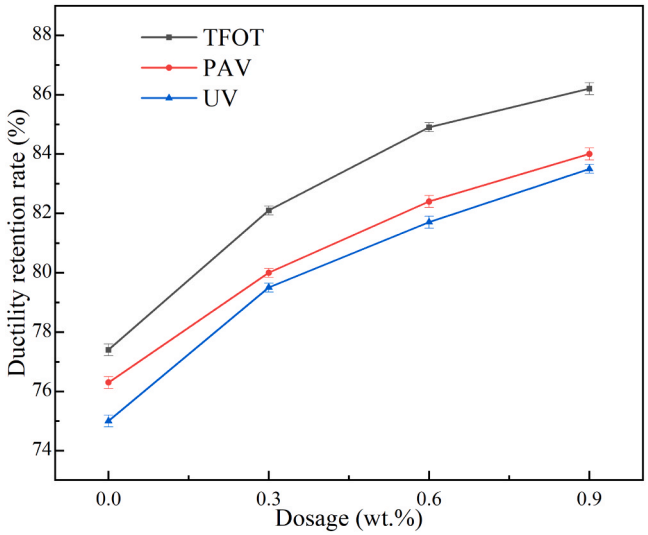

Fig. 13. DRR of DMA with varying dosages of DOPO.

$$PRR = \frac{Penetration_{after\ aging}}{Penetration_{before\ aging}} \times 100\% \quad (9)$$

Fig. 14 illustrated the PRR of DMA at different dosages of DOPO after TFOT, PAV, and UV aging. From the Fig. 14, the addition of DOPO significantly increased the PRR after DMA aging. The PRR of TFOT, PAV, and UV aged control asphalt were 77.6 %, 72.4 %, and 69.0 %, respectively, while the PRR of DMA containing 0.3 wt% DOPO was increased to 79.2 %, 75.5 %, and 71.4 %, respectively. This may also be attributed to the more stable components in DMA and the UV absorption ability of DOPO. As the dosage of DOPO increases, the PRR of DMA gradually increases. When the DOPO content was 0.6 wt%, the PRR of DMA after TFOT, PAV, and UV aging increased to 80.0 %, 77.1 %, and 72.6 %, respectively, while the DRR of DMA with 0.9 wt% DOPO content increased to 80.5 %, 78.0 %, and 73.3 % after TFOT, PAV, and UV aging, respectively. In summary, the higher the DOPO content, the better the anti-aging performance of DMA.

3.3.3. Rheological properties of DMA after aging

The aging resistance of DMA was assessed using Increase rate for G* and Reduction rate for δ before and after aging, with the following calculation formula:

$$Increase\ rate\ for G^* = \frac{G^*_{after\ aging} - G^*_{before\ aging}}{G^*_{before\ aging}} \times 100\% \quad (10)$$

$$Increase\ rate\ for\ \delta = \frac{\delta_{after\ aging} - \delta_{before\ aging}}{\delta_{before\ aging}} \times 100\% \quad (11)$$

Fig. 15 delineated the complex modulus (G*) and phase angle (δ)-temperature relationship for DMA with varying dosages of DOPO, following exposure to TFOT, PAV, and UV aging. In comparison with the unaged asphalt, a pronounced increase in G* was observed across all aged samples, accompanied by a reduction in δ, signifying a marked transition from viscous to elastic behavior as the asphalt underwent the aging process.

Post-TFOT aging, the DMA exhibited a complex modulus that bore resemblance to that of the unaltered control asphalt. However, subsequent exposure to PAV and UV aging showed a discernible reduction in the complex modulus of DMA, particularly when compared with the control sample. In the context of TFOT aging, the increase rate for G* for DMA augmented with 0.9 wt% DOPO exhibited a decrement of 33.68 % at 30 °C, paralleled by a 16.82 % decline in the reduction rate for δ. Upon PAV aging, the G* for DMA with 0.9 wt% DOPO manifested a 49.54 % decrease relative to the control asphalt at 30 °C, with reduction rate for δ curtailing by 23.36 %. Following UV aging, the G* for DMA enriched with 0.9 wt% DOPO diminished by 54.27 % at 30 °C in comparison to the control, while the δ for 0.9 wt% DMA receded by 37.25 %, underscoring the substantial anti-aging efficacy of DOPO on asphalt.

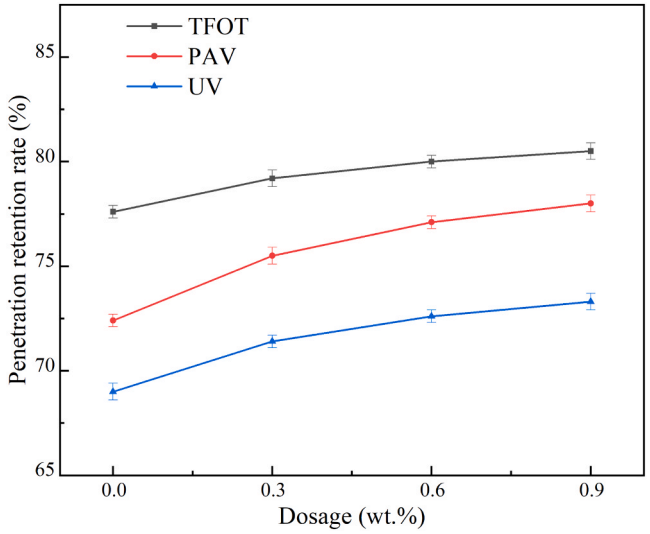

Fig. 14. PRR of DMA with varying dosages of DOPO.

3.3.4. FTIR Analysis

The chemical structural alterations in the asphalt were evaluated under the three aging conditions using FTIR spectroscopy, as illustrated in Fig. 16. The spectrum exhibits symmetric and antisymmetric vibrations of methylene (-CH) at approximately 2925 cm^{-1} and 2855 cm^{-1}. Additionally, due to the addition of DOPO, the absorption intensity of P-O and P═O stretching vibration peaks at 1200 cm^{-1} and 1057 cm^{-1} in DMA was widened. It was worth noting that after aging, absorption peaks of S═O absorption vibration and C═O absorption vibration appeared around 1030 cm^{-1} and 1700 cm^{-1}, respectively, with peak areas increasing relative to the degree of aging. In this research, the carbonyl index ($I_{C=O}$) and sulfoxide index ($I_{S=O}$) were employed to quantitatively assess the aging degree of asphalt [34]. The calculation formulas for $I_{C=O}$, $I_{S=O}$, $\Delta I_{C=O}$, and $\Delta I_{S=O}$ were presented in the equation.

$$I_{C=O} = \frac{A_{C=O}}{\Sigma A} \quad (12)$$

$$I_{S=O} = \frac{A_{S=O}}{\Sigma A} \quad (13)$$

$$\Delta I_{C=O} = I_{C=Oafter\ aging} - I_{C=Obefore\ aging} \quad (14)$$

$$\Delta I_{S=O} = I_{S=Oafter\ aging} - I_{S=Obefore\ aging} \quad (15)$$

where the peak area of C═O at 1700 cm^{-1} was represented by $A_{C=O}$, the peak area of S═O at 1030 cm^{-1} was represented by $A_{S=O}$, and the peak area of methylene at 2855 cm^{-1} and 2925 cm^{-1} was represented by A in the FTIR spectra. $\Delta I_{C=O}$ denoted the changes of $I_{C=O}$ under different aging conditions, while $\Delta I_{S=O}$ denoted the changes of $I_{S=O}$ under varying aging conditions.

The variation in the structural indexes of DAM and control asphalt under different aging conditions were shown in Table 3. In Table 3, Δ $I_{C=O}$ and Δ $I_{S=O}$ of DMA and control asphalt under three varying aging conditions underwent significant changes. Post- TFOT aging, the Δ $I_{C=O}$ and Δ $I_{S=O}$ indices for 0.9 wt% DMA were recorded at 0.017 and 0.008, respectively, showcasing a reduction of 0.015 and 0.06 when juxtaposed with the control asphalt. In the aftermath of PAV treatment, the Δ $I_{C=O}$ and Δ $I_{S=O}$ values for 0.9 wt% DMA stood at 0.023 and 0.017, respectively, underscoring a decrement of 0.018 and 0.011 compared to the control. These observed disparities were ascribed to the chemical interplay between DOPO and asphalt, a phenomenon further elucidated in our preliminary investigations. Therein, we discerned that DOPO interacts with unsaturated functional groups within the asphalt, fostering the formation of stable hydrocarbon and sulfide derivatives. This process inherently diminishes the prevalence of oxidation-prone groups, thereby curtailing the dosage of carbonyl and sulfoxide functionalities in the aged control asphalt.

Following ultraviolet (UV) aging, DMA accentuated an exemplary resistance against UV-induced degradation. The Δ $I_{C=O}$ and Δ $I_{S=O}$ values for 0.9 wt% DMA, post-UV aging, were observed at 0.026 and 0.020, respectively, which represented a substantial reduction of 0.029 and 0.021 in comparison to the control asphalt. Such variation was attributed not solely to the reactive interaction between DOPO and asphalt, culminating in more robust asphaltic components but also to the intrinsic proficiency in UV absorption of DOPO, offering a dual mechanism for its protective efficacy aging resistance.

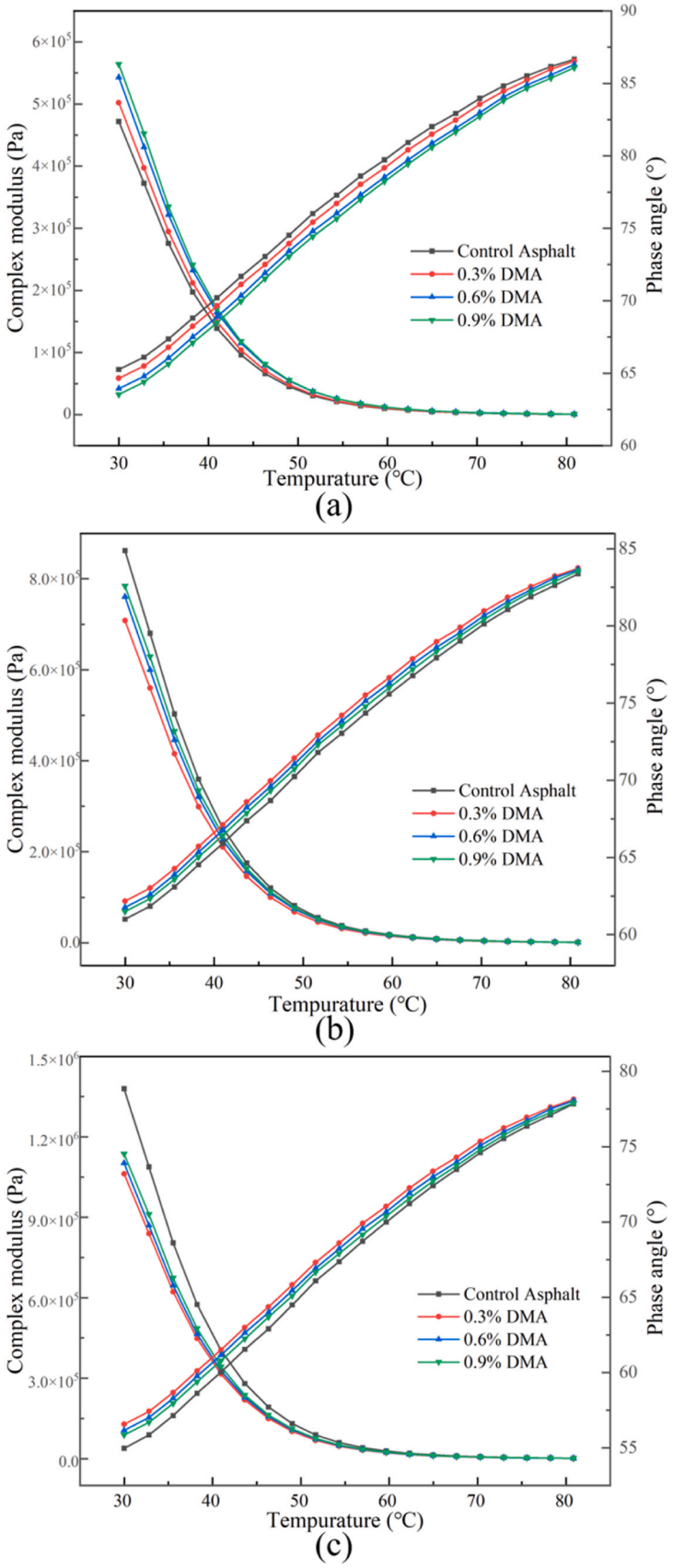

Fig. 15. Complex modulus and phase angle -temperature relationship of DMA with different dosages of DOPO after aging. (a) TFOT, (b) PAV, (c) UV.

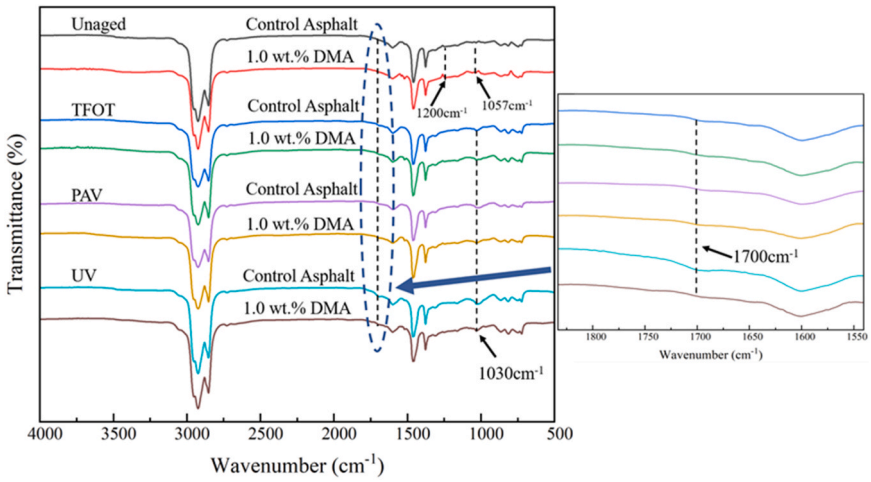

Fig. 16. FTIR spectra of control asphalt and DMA after TFOT, PAV and UV aging.

Table 3
The variation of structural indexes of control asphalt and DMA after aging.

Sample		$\Delta I_{C=O}$	$\Delta I_{S=O}$
Control Asphalt	TFOT	0.032	0.014
	PAV	0.041	0.028
	UV	0.055	0.041
0.9 wt% DMA	TFOT	0.017	0.008
	PAV	0.023	0.017
	UV	0.026	0.020

4. Conclusions

In this comprehensive investigation, the impact of varying dosage of DOPO on the chemical composition and structure, physical properties, rheological properties, and aging resistance of asphalt was meticulously examined. The ensuing insights have culminated in the following articulated conclusions:

Chemical Composition Analysis: The ^{1}H NMR spectroscopic evaluation disclosed a progressive diminution in the H_α content, concomitant with an elevation in the H_β and H_γ content. This trend elucidated a chemical interaction between DOPO and the unsaturated functional moieties inherent in the asphalt. Furthermore, the analysis of asphalt composition revealed a reduction in the saturates in DMA while documenting an escalation in the aromatics and resins, thereby indicating the transformation of saturates within the asphalt into aromatic and resin under the influence of DOPO.

High-Temperature Performance Enhancement: The integration of DOPO into the asphalt had markedly augmented its high-temperature operational characteristics. Relative to the control asphalt, an escalation in DOPO dosage had notably enhanced the softening point, viscosity, and rutting parameter of the DMA, while the alterations in penetration and ductility remained marginal. This phenomenon was ascribed to the transmutation of certain reactive saturates in DMA into aromatics and resins, albeit the proportion of stable saturates and asphaltenes remained unaltered.

The comparative analysis of physical and rheological properties of DMA, alongside its functional groups before and after undergoing TFOT, PAV, and UV aging processes, signified that DOPO incorporation had bolstered the material's resistance to aging. In contrast to the control asphalt, post-aging analyses revealed a significant reduction in SPI, VAI, complex modulus, carbon, and sulfur indices in DMA, while the DRR and PRR values exhibited an increase. This improvement is attributed to the reaction between DOPO and the aging unsaturated functional groups in asphalt to generate more stable aromatics and resins, thereby improving the aging resistance of DMA

UV Aging Resistance: When juxtaposed with TFOT and PAV aging, DMA demonstrated a more pronounced decrement in SPI, VAI, and complex modulus, in tandem with an amplification in DRR and PRR post-UV aging. The most notable decline was observed in the carbonyl and sulfoxide indices after UV exposure, which was attributed to the reaction between DOPO and the volatile or reflected saturated components in asphalt to generate stable aromatic and gum compounds, and DOPO had excellent UV absorption ability.

Optimum dosage: Considering the performance effect, efficiency of fume suppression and cost of DOPO on asphalt, the optimal dosage of DOPO in asphalt was 0.6 wt%.

Recommendations

The research on the influence of DOPO on the performance of asphalt from different oil sources is significance for further optimization of reactive flue gas inhibitor systems. In our future research, we will explore the impact of DOPO on the performance of asphalt from different oil sources and evaluate the sustainability of DOPO modified asphalt.

CRediT authorship contribution statement

Hao Duan: Data curation. **Yanheng He:** Methodology. **Shi Xu:** Methodology, Formal analysis. **Tianwei Zhang:** Methodology. **Shangheng Zeng:** Writing – review & editing, Writing – original draft, Investigation, Data curation. **Jianying Yu:** Writing – review & editing, Data curation.

Declaration of Competing Interest

The authors declare that they have no known competing financial interests or personal relationships that could have appeared to influence the work reported in this paper.

Data availability

Data will be made available on request.

Acknowledgements

This work was supported by the Science and Technology Project of Petro China Co. Ltd (No. RLY-2023Y-03) and the National Key R&D Program of China (No. 2022YFC3801600). The authors gratefully acknowledge their financial support.

References

[1] Y.F. Pei, Y.C. Guo, A.Q. Shen, S.C. Mao, Uniformity evaluation of asphalt pavements in hot and humid areas based on ground-penetrating radar, Constr. Build. Mater. 384 (2023), https://doi.org/10.1016/j.conbuildmat.2023.131432.

[2] F. Ma, C. Li, Z. Fu, Y. Huang, J.S. Dai, Q. Feng, Evaluation of high temperature rheological performance of polyphosphoric acid-SBS and polyphosphoric acid-crumb rubber modified asphalt, Constr. Build. Mater. 306 (2021), https://doi.org/10.1016/j.conbuildmat.2021.124926.

[3] X. Jiang, F. Zhang, B. Huang, H. Titi, P. Polaczyk, Y. Ma, Y. Wang, Z. Cheng, Full-scale accelerated testing of geogrid-reinforced inverted pavements, Geotext. Geomembr. 52 (2024), https://doi.org/10.1016/j.geotexmem.2024.01.005.

[4] H. Sivilevicius, J. Braziunas, O. Prentkovskis, Technologies and Principles of hot recycling and investigation of preheated reclaimed asphalt pavement batching process in an asphalt mixing plant, Appl. Sci. -Basel 7 (11) (2017), https://doi.org/10.3390/app7111104.

[5] Z.S. Ge, H. Li, Z.T. Han, Q.S. Zhang, Properties of cold mix asphalt mixtures with reclaimed granular aggregate from crushed PCC pavement, Constr. Build. Mater. 77 (2015) 404–408, https://doi.org/10.1016/j.conbuildmat.2014.12.084.

[6] Z.H. Al-Saffar, H. Yaacob, M. Satar, M.K. Saleem, J.C. Lai, R.P. Jaya, A review on rejuvenating materials used with reclaimed hot mix asphalt, Can. J. Civ. Eng. 48 (3) (2021) 233–249, https://doi.org/10.1139/cjce-2019-0635.

[7] B.C. Zhou, G.Y. Gong, Y. Liu, M.Y. Guo, C. Wang, Technical and environmental performance assessment of VOCs inhibited asphalt binders and mixtures, Transp. Res. Part D. -Transp. Environ. 124 (2023), https://doi.org/10.1016/j.trd.2023.103931.

[8] L.P. Thives, E. Ghisi, Asphalt mixtures emission and energy consumption: a review, Renew. Sustain. Energy Rev. 72 (2017) 473–484, https://doi.org/10.1016/j.rser.2017.01.087.

[9] Z.L. Cao, G.Y. Gong, Y. Liu, X.J. Cao, B.M. Tang, C. Wang, Effects of different inhibitors on emission characteristics, environmental impact and health risk of volatile organic compounds from asphalt binder, J. Clean. Prod. 428 (2023), https://doi.org/10.1016/j.jclepro.2023.139427.

[10] X. Jiang, H.H. Zhu, Z.G. Yan, F.S. Zhang, X.Y. Huang, Z. Leng, C.Q. Yan, N. Hua, D. Lu, X.H. Zhang, R. Xiao, Fire-retarding asphalt pavement for urban road tunnels: a state-of-the-art review and beyond, Fire Technol. (2024), https://doi.org/10.1007/s10694-024-01556-2.

[11] G.C. Wang, X.L. Yang, D.Y. Yang, H.L. Rong, Y.J. Meng, G.Y. Liu, Effect of heating history on the emission of volatile organic compounds from asphalt materials, Sci. Total Environ. 900 (2023), https://doi.org/10.1016/j.scitotenv.2023.165692.

[12] S.C. Mo, Y.H. Wang, F. Xiong, C.J. Ai, Effects of asphalt source and mixing temperature on the generated asphalt fumes, J. Hazard. Mater. 371 (2019) 342–351, https://doi.org/10.1016/j.jhazmat.2019.03.025.

[13] Y.J. Boom, D.L. Xuan, M. Enfrin, M. Swaney, H. Masood, B.K. Pramanik, D. Robert, F. Giustozzi, Engineering properties, microplastics and emissions assessment of recycled plastic modified asphalt mixtures, Sci. Total Environ. 893 (2023), https://doi.org/10.1016/j.scitotenv.2023.164869.

[14] C.J. Spreadbury, K.A. Clavier, A.M. Lin, T.G. Townsend, A critical analysis of leaching and environmental risk assessment for reclaimed asphalt pavement management, Sci. Total Environ. 775 (2021), https://doi.org/10.1016/j.scitotenv.2021.145741.

[15] X.M. Xie, C.R. Hao, Y. Huang, Z. Huang, Influence of TiO_2-based photocatalytic coating road on traffic-related NO_x pollutants in urban street canyon by CFD modeling, Sci. Total Environ. 724 (2020), https://doi.org/10.1016/j.scitotenv.2020.138059.

[16] R. Wu, Y. Xiao, P.F. Zhang, J.T. Lin, G. Cheng, Z.W. Chen, R. Yu, Asphalt VOCs reduction of zeolite synthesized from solid wastes of red mud and steel slag, J. Clean. Prod. 345 (2022), https://doi.org/10.1016/j.jclepro.2022.131078.

[17] D. Lu, X. Jiang, Z. Tan, B. Yin, Z. Leng, J. Zhong, Enhancing sustainability in pavement Engineering: a-state-of-the-art review of cement asphalt emulsion mixtures, Clean. Mater. 9 (2023), https://doi.org/10.1016/j.clema.2023.100204.

[18] Y. Xiao, M. Wan, K.J. Jenkins, S.P. Wu, P.Q. Cui, Using activated carbon to reduce the volatile organic compounds from bituminous materials, J. Mater. Civ. Eng. 29 (10) (2017), https://doi.org/10.1061/(asce)mt.1943-5533.0002024.

[19] T. Bubeníková, M. Bednár, T. Gergel, R. Igaz, Adsorption effect of added powder graphite on reduction of volatile organic compounds emissions from expanded polystyrene, Bioresources 14 (4) (2019) 9729–9738, https://doi.org/10.15376/biores.14.4.9729-9738.

[20] Y. Lv, S.P. Wu, N. Li, P.D. Cui, H. Wang, S. Amirkhanian, Z.G. Zhao, Performance and VOCs emission inhibition of environmentally friendly rubber modified asphalt with UiO-66 MOFs, J. Clean. Prod. 385 (2023), https://doi.org/10.1016/j.jclepro.2022.135633.

[21] N. Tang, K.K. Yang, Y. Alrefaei, J.G. Dai, L.M. Wu, Q. Wang, Reduce VOCs and PM emissions of warm-mix asphalt using geopolymer additives, Constr. Build. Mater. 244 (2020), https://doi.org/10.1016/j.conbuildmat.2020.118338.

[22] H.S. Liang, S.M. Song, X.F. Liu, F.Y. Sun, Z.H. Cao, Y.F. Liu, Y.F. Ren, X. Li, Study on the inhibition effect and mechanism of basic zinc carbonate composite asphalt fumes suppressant, Constr. Build. Mater. 416 (2024), https://doi.org/10.1016/j.conbuildmat.2024.135220.

[23] S. Li, Q. Liu, H. Wang, J. Wang, L. He, S. Wu, Effect of kaolin and sepiolite on fume emissions of rubber modified asphalt, Constr. Build. Mater. 416 (2024), https://doi.org/10.1016/j.conbuildmat.2024.135276.

[24] S.H. Zeng, X.Y. Gong, X.B. Han, S. Xu, J.H. Xu, X. Li, J.Y. Yu, Effect of organic attapulgite on properties of SBS modified asphalt waterproofing membranes, Constr. Build. Mater. 360 (2022), https://doi.org/10.1016/j.conbuildmat.2022.129606.

[25] S.P. Mao, S.H. Zeng, Z.Y. Li, X.B. Han, J.Y. Yu, Effects of solvent-free bentonite fluid on physical, rheological and aging properties of SBS modified bitumen, Case Stud. Constr. Mater. 19 (2023), https://doi.org/10.1016/j.cscm.2023.e02590.

[26] W.H. Dong, F. Ma, C. Li, Z. Fu, Y. Huang, J. Liu, Evaluation of anti-aging performance of biochar modified asphalt binder, Coatings 10 (11) (2020), https://doi.org/10.3390/coatings10111037.

[27] L.P. Cao, C. Yang, A. Li, P. Wang, Y. Zhang, Z.J. Dong, Flue gas composition of waste rubber modified asphalt (WRMA) and effect of deodorants on hazardous constituents and WRMA, J. Hazard. Mater. 403 (2021), https://doi.org/10.1016/j.jhazmat.2020.123814.

[28] S.H. Zeng, S.P. Mao, S. Xu, Y.H. He, J.Y. Yu, Investigation on DOPO as reactive fumes suppressant to reduce the fumes emission of asphalt, J. Hazard. Mater. 463 (2024), https://doi.org/10.1016/j.jhazmat.2023.132878.

[29] Y.Y. Zhou, Y.C. Lin, B. Tawiah, J. Sun, R.K.K. Yuen, B. Fei, DOPO-Decorated two-dimensional MXene nanosheets for flame-retardant, ultraviolet-protective, and reinforced polylactide composites, Acs Appl. Mater. Interfaces 13 (18) (2021) 21876–21887, https://doi.org/10.1021/acsami.1c05587.

[30] Q.X. Dong, Y.F. Ding, B. Wen, F. Wang, H.C. Dong, S.M. Zhang, T.X. Wang, M. S. Yang, Improvement of thermal stability of polypropylene using DOPO-immobilized silica nanoparticles, Colloid Polym. Sci. 290 (14) (2012) 1371–1380, https://doi.org/10.1007/s00396-012-2631-0.

[31] Z.G. Zhao, S.P. Wu, Q.T. Liu, C. Yang, Y.X. Zou, P. Wan, Feasibility assessment of CeO_2 nanoparticles as aging-resistant agent of asphalt, Constr. Build. Mater. 330 (2022), https://doi.org/10.1016/j.conbuildmat.2022.127245.

[32] Z.J. Pu, L.S. Zou, F. Wu, X. Wang, Q.X. Peng, J.C. Zhong, X.B. Liu, Y.L. Wang, Y. K. Pan, D.Y. Jiang, Z.P. Ning, Preparation of phosphorus-nitrogen flame retardant DOPO-DBAPh and its flame retarded epoxy-based composites, J. Vinyl Addit. Technol. 30 (2) (2024) 398–409, https://doi.org/10.1002/vnl.22055.

[33] K.P. Qin, X. Zhang, Y. Xu, Y.Y. Pang, Z.J. Wang, Y.F. Liu, W.G. Zheng, A Creative approach to prepare a macromolecular flame retardant with flexibility: DOPO-modified epoxidized polybutadiene, Acs Appl. Polym. Mater. 3 (10) (2021) 4896–4903, https://doi.org/10.1021/acsapm.1c00681.

[34] X.D. Hou, S.T. Lv, Z. Chen, F.P. Xiao, Applications of Fourier transform infrared spectroscopy technologies on asphalt materials, Measurement 121 (2018) 304–316, https://doi.org/10.1016/j.measurement.2018.03.001.